JOURNAL OF COMPUTATIONAL PHYSICS 111, 354–372 (1994)

An Approximate Riemann Solver for Ideal Magnetohydrodynamics

WENLONG DAI AND PAUL R. WOODWARD

School of Physics and Astronomy, Supercomputer Institute, Army High Performance Computing Research Center, University of Minnesota, Minneapolis/St. Paul, Minnesota 55415

Received July 6, 1992; revised August 25, 1993

To construct numerical schemes of the Godunov type for solving magnetohydrodynamical (MHD) problems, an approximate method of solving the MHD Riemann problem is required in order to calculate the time-averaged fluxes at the interfaces of numerical zones. Such an MHD Riemann solver is presented here which treats all waves emanating from the initial discontinuity as themselves discontinuous. Thus shock jump conditions are used for rarefactions, which limits the applicability of this work to weak rarefactions, the case most important for computation. The solutions from our approximate MHD Riamnn solver consist of two fast waves (either shock or rarefaction) two rotational discontinuities, two rarefaction waves (either shock or rarefaction), and one contact discontinuity for a general MHD Riemann problem. In order to display rotational discontinuities, a three-component model is necessary. Only under very limited circumstances is there no rotational discontinuity involved and thus the two component approximation may be used in the MHD Riemann problem. The solutions of the MHD Riemann problem in the shock tube problem which generates the compound wave in the earlier work contain two fast rarefaction waves, two slow shocks, one contact discontinuity, and one rotational discontinuity in our formalism.

1. INTRODUCTION

During the last three decades, highly efficient numerical schemes for the conservation laws of hydrodynamics have been developed. Among them, Godunov-type schemes are considered to be particularly efficient for many problems, especially for shock dynamics. Examples of the Godunov-type schemes are Godunov's scheme [1], the MUSCL scheme [2, 3, 9] and its successor PPM [4, 7, 8], Roe's scheme [5], Harten's TVD scheme [6], and the ENO schemes [10–12]. It is natural to extend what we know to be efficient and sufficiently accurate in hydrodynamics to magnetohydrodynamics (MHD). Several investigators have worked on the development of high-order Godunov-type schemes for MHD (Giz [13], Giz and Woodward [21], Brio and Wu [16], Zachary and Colella [22]). Giz and Woodward have developed an approach useful only for MHD shocks of modest strength. Brio and Wu [16] have developed a high-resolution method for MHD based on a Roe-type approach, but their technique requires the ratio of the specific heats $\gamma = 2$ to perform the analytic flux difference splitting. Zachary and Colella [22] have applied an extension [19] of the Engquist–Osher flux to the MHD equations to develop a technique for a solution of the MHD Riemann problem. (Our work was concurrent with that reported in their note [22].) The MHD Riemann solver presented below is intended for use in problems which involve strong nonlinear waves.

Thus we consider conservation laws,

$$\frac{\partial \mathbf{U}}{\partial t} + \frac{\partial \mathbf{F}(\mathbf{U})}{\partial x} = 0, \tag{1}$$

and their discretized form,

$$\langle \mathbf{U} \rangle_N = \langle \mathbf{U} \rangle + \frac{\Delta t}{\Delta x} (\bar{\mathbf{F}}_L - \bar{\mathbf{F}}_R).$$

Here $\mathbf{U}$ *is a vector which represents a set of variables and* $\mathbf{F}(\mathbf{U})$ represents the associated flux vector. $\langle \mathbf{U} \rangle$ is the old zone-averaged value of vector $\mathbf{U}$, and $\langle \mathbf{U} \rangle_N$ is its updated value. $\bar{\mathbf{F}}_L$ is the time-averaged flux over the time step Δt at the left boundary of the current zone; $\bar{\mathbf{F}}_R$ is the time-averaged flux at the right boundary of the zone. The discretized form of Eq. (1) is exact. A Godunov-type approximation can be viewed as a means of constructing from the zone averages $\langle \mathbf{U} \rangle$ appropriate left and right states $\mathbf{U}_{LL}$ and $\mathbf{U}_{RL}$ from which the flux $\bar{\mathbf{F}}_L$ may be approximated by solving the corresponding Riemann problem. Thus the Riemann problem is the key ingredient in this type of schemes.

In [7] by Woodward and Colella, an extensive comparison of various numerical methods for shock hydrodynamics was made and it was found that the most accurate one of the methods tested there was the piecewise-parabolic method (PPM), developed by Woodward and Colella. In this paper the same technique is used in that all the waves emanating from the initial discontinuity are treated as discontinuous jumps. Since this technique works for shock dynamics quite well, we expect it to work for

0021-9991/94 $6.00

MHD in the most important applications, weak rarefactions. Thus the basic idea of the approximate Riemann solver in PPM is used and the special procedures for the MHD case are presented in this paper.

Since the MHD equations form a nonstrictly hyperbolic system, and even a nonconvex system [16], the wave structure is more complicated than that in hydrodynamics. Much attention has been devoted to the hyperbolicity and nonconvexity of the MHD system (Glimm [18] and that spatial conference proceedings). One conclusion drawn from the nonconvexity is the existence of the compound wave consisting of a shock and attached to it a rarefaction wave of the same family as shown by Brio and Wu [16] (see Fig. 1). In this paper, we will show that the solutions of the MHD Riemann problem in the shock tube problem which generate the compound wave in the earlier work, contains a rotational discontinuity in our formalism. We find that the solutions for a typical MHD Riemann problem contains two fast waves (either shock or rarefaction), two slow waves (either shock or rarefaction), two rotational discontinuities, and one contact discontinuity.

Our main concern for the Riemann solver is that it produces a reasonable solution obeying all conservation laws for any pair of left and right states and including all the kinds of discontinuities in ideal MHD. It is intended to be used mainly for the calculation of time-averaged fluxes at the interfaces of numerical zones for a Godunov-type scheme. Problems possibly arising from non-strict hyperbolicity or non-convexity will be handled through the discretization of the conservation law Eq. (1) on the grid. This will represent any compound waves over several grid zones. Problems resulting from degenerate wave speeds for which different results are obtained depending upon the ratio of infinitesimal transport coefficients must also be handled by adding appropriate physical and/or numerical dissipation terms to the computer code beyond the Riemann solver.

A one-dimensional system described by ideal MHD equations permits Alfven waves as well as fast and slow MHD waves generally. Associated with these three kinds of waves,

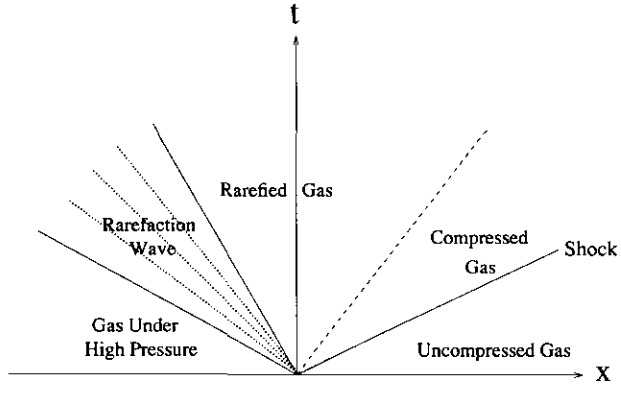

FIG. 1. Waves produced in a shock tube.

three kinds of discontinuities, fast shocks, rotational discontinuities, and slow shocks, are allowed to exist in the ideal MHD besides contact discontinuities. All the discontinuities allowed to exist in the system have been taken into consideration in this paper. Thus the Riemann solver to be presented in this paper includes interactions among the all discontinuities in the ideal MHD.

The plan of this paper is as follows. In the second section, MHD equations in a Lagrangian mass coordinate are introduced. In the third section, we give a linear Riemann solver similar to that developed by Giz [13] for a Godunov method (cf. [1]), which may be used in the first step in the nonlinear Riemann solver. General jump conditions for all the discontinuities are presented at the beginning of the fourth section, and the properties of the rotational discontinuities and MHD shocks are investigated there. The procedures for an approximate nonlinear Riemann solver are constructed in the fifth section. A summary of this work and brief discussions are given in the final section of this paper.

2. MHD EQUATIONS

The ideal MHD equations characterize the flow of a conducting fluid in the presence of a magnetic field. They represent the coupling of fluid dynamical equations with Maxwell's equations of electrodynamics. By neglecting displacement current, electrostatic force, effects of viscosity, resistivity, and heat conduction, one obtains the following ideal MHD equations (see Landau and Lifshits [23]):

$$\frac{\partial \rho}{\partial t} + \nabla \cdot (\rho \mathbf{u}) = 0,$$

$$\rho \left(\frac{\partial \mathbf{u}}{\partial t} + \mathbf{u} \cdot \nabla \mathbf{u} \right) = -\nabla p + \frac{1}{4\pi} (\nabla \times \mathbf{B}) \times \mathbf{B},$$

$$\frac{\partial}{\partial t} \left(\frac{1}{2} \rho \mathbf{u}^2 + \rho \varepsilon + \frac{1}{8\pi} \mathbf{B}^2 \right) = -\nabla \cdot \mathbf{q},$$

$$\frac{\partial \mathbf{B}}{\partial t} = \nabla \times (\mathbf{u} \times \mathbf{B}).$$

Here ρ is the density, $\mathbf{u}$ the flow velocity, $\mathbf{B}$ the magnetic field, p the thermal pressure, ε the internal energy of the fluid, and $\mathbf{q}$ is the energy flux defined as

$$\mathbf{q} \equiv \rho \mathbf{u} \left(\frac{1}{2} \mathbf{u}^2 + \varepsilon + \frac{1}{\rho} p \right) + \frac{1}{4\pi} \mathbf{B} \times (\mathbf{u} \times \mathbf{B}).$$

The magnetic field satisfies the divergence-free condition, and the thermal pressure is related to the internal energy through the gamma-law equation of state $p = (\gamma - 1) \rho \varepsilon$. The Lagrangian equivalents of these Eulerian MHD equations can be obtained by introducing $d/dt \equiv (\partial/\partial t + \mathbf{u} \cdot \nabla)$.

We introduce a Lagrangian mass coordinate $\mathbf{m}$ by the relation $d\mathbf{m} \equiv \rho\, d\mathbf{x}$, and write the MHD equations in the mass coordinate:

$$\frac{dV}{dt} - \nabla_m \cdot \mathbf{u} = 0,$$

$$\frac{d\mathbf{u}}{dt} + \nabla_m \cdot \mathbf{P} = 0,$$

$$\frac{dE}{dt} + \nabla_m \cdot (\mathbf{P} \cdot \mathbf{u}) = 0,$$

$$\frac{d}{dt}(V\mathbf{B}) - \nabla_m \cdot (\mathbf{u}) = 0.$$

Here V is the specific volume of the fluid, $\mathbf{P}$ is the total pressure tensor including the magnetic field, and E is the specific total energy. They are defined as

$$\mathbf{P} \equiv \left(p + \frac{\mathbf{B}^2}{8\pi}\right)\mathbf{I} - \frac{1}{4\pi}\mathbf{BB},$$

$$E \equiv \frac{1}{2}\mathbf{u}^2 + \varepsilon + \frac{1}{8\pi\rho}\mathbf{B}^2.$$

In this paper we will construct an approximate Riemann solver for use in numerical methods which employ directional operator splitting. Therefore we will restrict our attention to the one-dimensional MHD equations which are obtained from the MHD equations in the mass coordinate by assuming that all variables depend on x and t only. The resulting equations are

$$\frac{dV}{dt} = \frac{\partial u_x}{\partial m}, \tag{2.1}$$

$$\frac{du_x}{dt} = -\frac{\partial P}{\partial m}, \tag{2.2}$$

$$\frac{du_y}{dt} = -\frac{\partial \Lambda_y}{\partial m}, \tag{2.3}$$

$$\frac{du_z}{dt} = -\frac{\partial \Lambda_z}{\partial m}, \tag{2.4}$$

$$\frac{d}{dt}(VB_y) = \frac{\partial}{\partial m}(B_x u_y), \tag{2.5}$$

$$\frac{d}{dt}(VB_z) = \frac{\partial}{\partial m}(B_x u_z), \tag{2.6}$$

$$\frac{dE}{dt} = -\frac{\partial}{\partial m}(Pu_x + \Lambda_y u_y + \Lambda_z u_z). \tag{2.7}$$

Here the mass coordinate m is simplified to $dm = \rho\, dx$ and any symbol with the subscript x (or y or z) is the x (or y or z) component of the variable. The longitudinal part of the magnetic field B_x is a constant, and P, Λ_y, and Λ_z are defined by the following equations:

$$P \equiv p + \frac{1}{8\pi}(B_y^2 + B_z^2 - B_x^2),$$

$$\Lambda_y \equiv -\frac{1}{4\pi} B_x B_y,$$

$$\Lambda_z \equiv -\frac{1}{4\pi} B_x B_z.$$

It is well known that this system permits Alfven waves, fast waves, and slow waves. It should be pointed out that Alfven waves do not occur generally if we demand that $u_z = 0$ and $B_z = 0$. Thus, in order to take into consideration Alfven waves and their associated rotational discontinuities, we have to treat the full equations (2.1)–(2.7).

3. A LINEAR RIEMANN SOLVER

Interactions involving shocks are rarefactions in a tube filled with gas (a "shock tube") were studied by Riemann more than one hundred years ago. The MHD Riemann problem is the initial value problem, Eqs. (2.1)–(2.7), subject to a specified initial condition:

$$\mathbf{U}_0(x) = \begin{cases} \mathbf{U}_L & (x < 0), \\ \mathbf{U}_R & (x > 0). \end{cases}$$

Here $\mathbf{U}_L$ and $\mathbf{U}_R$ are any given left state and right state, and they are completely specified by seven variables, V, p, u_x, u_y, u_z, B_y, and B_z and three constants, the ratio of the specific heats γ, gas constant R, and the longitudinal component of the magnetic field B_x.

With increasing time beyond zero, the discontinuity between the initial left and right states will break into leftward and rightward moving waves which are separated by a constant surface. Each wave can be either a shock or a rarefaction wave or a rotational discontinuity, depending on the initial data. It is possible to have a discontinuity across each wave front. Thus six wave fronts corresponding to the three waves in each direction and a contact surface separate the whole $(m-t)$ (or $(x-t)$) plane into eight possibly different regions. We label them R1, R2, R3, R4, R5, R6, R7, and R8, respectively, as in Fig. 2. The states in the regions R1 and R8 are the left and right states, respectively. The Riemann problem is to determine the types of waves, their strengths, and their speeds, and the flow properties in the other six regions. The algorithm for determining the solution of this problem is called a Riemann solver in MHD.

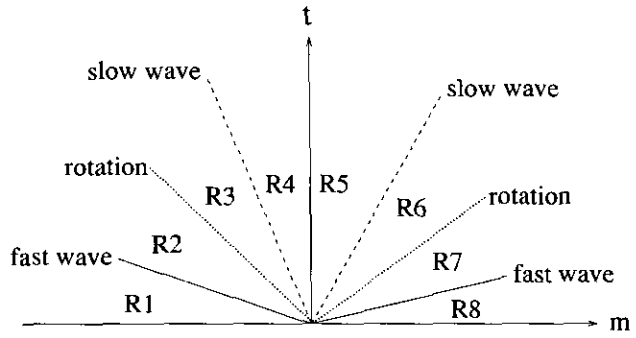

FIG. 2. All possible waves generated from a MHD Riemann problem and eight possibly different states divided by the wave fronts.

As an introductory step to the approximate nonlinear Riemann solver which we will construct in the fifth section, we first construct a linearized approximate Riemann solver. Following the steps in the book by Courant and Friedrichs [24], we first write Eqs. (2.1)–(2.7) in the form

$$\frac{d\mathbf{U}}{dt} + A\frac{\partial \mathbf{U}}{\partial m} = 0.$$

Here A is a 7×7 matrix, which can be obtained with no difficulty. From the eigenvalues of the matrix A, one may obtain the nonlinear wave speeds in the mass coordinate for Alfven waves, fast waves, and slow waves, C_a, C_f, and C_s, i.e.,

$$C_a^2 = C_x^2,$$
$$C_{f,s}^2 = \tfrac{1}{2}[(C_0^2 + C_x^2 + C_t^2) \pm \sqrt{(C_0^2 + C_x^2 + C_t^2)^2 - 4C_0^2 C_x^2}].$$

Here C_0, C_x, and C_t are defined as

$$C_0 \equiv \sqrt{\gamma p \rho},$$
$$C_x \equiv \sqrt{\rho B_x^2/(4\pi)},$$
$$C_t \equiv \sqrt{\rho(B_y^2 + B_z^2)/(4\pi)}.$$

The plus sign is for fast waves and the minus sign for slow waves. Besides these eigenvalues, there is a zero-eigenvalue, which is the propagation speed for entropy disturbances in the fluid in the Lagrangian coordinate.

Each wave speed C in either direction defines a characteristic in the $m-t$ plane:

$$\frac{dm}{dt} = C.$$

Corresponding to each characteristic, there is a Riemann invariant R associated with it, which is conserved along the characteristic, i.e.,

$$dR = 0 \qquad \text{along} \quad \frac{dm}{dt} = C.$$

The Riemann invariant R_0 associated with the zero-eigenvalue is related to the specific entropy of the gas:

$$R_0 = pV^{\gamma}.$$

The remaining six Riemann invariants may be expressed only as inexact differentials:

$$dR_{f\pm} \equiv (C_f^2 - C_x^2)(dP \pm C_f\, du_x) + \rho A_y(dA_y \pm C_f\, du_y) + \rho A_z(dA_z \pm C_f\, du_z)$$
$$= 0 \qquad \text{along} \quad \frac{dm}{dt} = \pm C_f,$$

$$dR_{s\pm} \equiv (C_s^2 - C_x^2)(dP \pm C_s\, du_x) + \rho A_y(dA_y \pm C_s\, du_y) + \rho A_z(dA_z \pm C_s\, du_z)$$
$$= 0 \qquad \text{along} \quad \frac{dm}{dt} = \pm C_s,$$

$$dR_{a\pm} \equiv \pm C_a(B_z\, du_y - B_y\, du_z) - \frac{1}{4\pi} B_x(B_z\, dB_y - B_y\, dB_z)$$
$$= 0 \qquad \text{along} \quad \frac{dm}{dt} = \pm C_a.$$

Fortunately, for numerical computations, only differences of Riemann invariants will be required.

The directions of the characteristics are determining factors in discussing the dependence of the solution on the given initial data. Consider any point A in the $(m-t)$-plane, and draw the seven characteristics $L_{f\pm}$, $L_{s\pm}$, $L_{a\pm}$, and L_0 through the point A until they intersect the m-axis, see Fig. 3. The interval from A_{f+} to A_{f-} on the m-axis is the domain of dependence of the point A. Any disturbance of the initial data outside of this interval does not influence the values at the point A. The disturbance of the initial data in the domain of dependence is by no means confined to infinitesimal amplitude. The only restriction we will impose

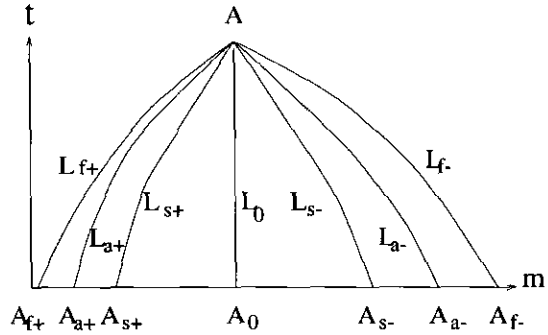

FIG. 3. The domains of dependence for MHD fast waves, slow waves and Alfven waves. $L_{f\pm}$ are the characteristics for two fast waves, $L_{s\pm}$ for the two slow waves, and $L_{a\pm}$ for the two Alfven waves.

in this section is that the flows are assumed to be continuous.

Since the Riemann invariants are constants along their own characteristics, we can construct the states in each of the six regions using the Riemann invariants by assuming that the invariants do not change when they cross the other characteristics. This assumption is true only for continuous flows. Under this assumption, the Riemann invariants R_{f+}, R_{a+}, R_{s+}, R_0, R_{s-}, R_{a-}, and R_{f-} at the point A have the same values as those at the points A_{f+}, A_{a+}, A_{s+}, A_0, A_{s-}, A_{a-}, and A_{f-}, respectively (see Fig. 4).

Since we have constant left and right states and the jump between them is assumed to be small in this section, all characteristics of the same family starting from the left (or from the right) of A_0 can be considered to be parallel straight lines. Thus the state in the region R4 can be calculated from the conservation of the Riemann invariants along their characteristics. For example, we have the following set of equations for the state $\{U_i, i=1, 2, ..., 7\}$ in region R4:

$$\sum_{i=1}^{i=7} \alpha_{i\mathrm{L}}^{(f+)}(U_i - U_{i\mathrm{L}}) = 0,$$

$$\sum_{i=1}^{i=7} \alpha_{i\mathrm{L}}^{(a+)}(U_i - U_{i\mathrm{L}}) = 0,$$

$$\sum_{i=1}^{i=7} \alpha_{i\mathrm{L}}^{(s+)}(U_i - U_{i\mathrm{L}}) = 0,$$

$$\sum_{i=1}^{i=7} \alpha_{i\mathrm{L}}^{(0)}(U_i - U_{i\mathrm{L}}) = 0,$$

$$\sum_{i=1}^{i=7} \alpha_{i\mathrm{R}}^{(s-)}(U_i - U_{i\mathrm{R}}) = 0,$$

$$\sum_{i=1}^{i=7} \alpha_{i\mathrm{R}}^{(a-)}(U_i - U_{i\mathrm{R}}) = 0,$$

$$\sum_{i=1}^{i=7} \alpha_{i\mathrm{R}}^{(f-)}(U_i - U_{i\mathrm{R}}) = 0.$$

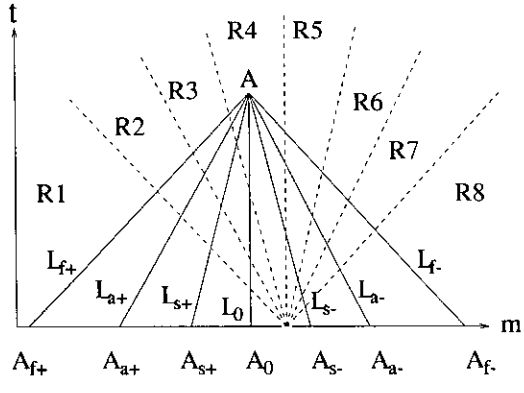

FIG. 4. The procedures to find the state in region R4 in a linear MHD Riemann solver.

Here coefficient $\alpha_i^{(f+)}$ is that in the differential dR_{f+} if we write it as

$$dR_{f+} = \sum_{i=1}^{i=7} \alpha_i^{(f+)}\, dU_i,$$

and the remaining coefficients have the similar meanings for each Riemann invariant, respectively. The subscript "L" (or "R") stands for the evaluation at the left (or right) state.

This linear Riemann solver is accurate only in the limit of weak wave disturbances, but it can be used for the initial guess for weak discontinuities.

To complete the discussion, we give the Riemann invariants for the specific cases with vanishing transverse or longitudinal part of the magnetic field. For vanishing transverse components of the field, we have

$$dR_{1\pm} = 0 \qquad \text{along} \quad \frac{dm}{dt} = \pm C_0,$$

$$dR_{2,3\pm} = 0 \qquad \text{along} \quad \frac{dm}{dt} = \pm C_x,$$

with the definitions

$$dR_{1\pm} \equiv [dP] \pm C_0\, du_x,$$
$$dR_{2\pm} \equiv dA_y \pm C_x\, du_y,$$
$$dR_{3\pm} \equiv dA_z \pm C_x\, du_z.$$

For the vanishing longitudinal component of the magnetic field, we have

$$dR_{\pm} = 0 \qquad \text{along} \quad \frac{dm}{dt} = \pm C_{ms}$$

with the definitions

$$C_{ms} \equiv \sqrt{C_0^2 + C_t^2},$$
$$dR_{\pm} \equiv [dP] \pm C_{ms}\, du_x.$$

4. DISCONTINUITIES

As we know, initial discontinuities are sometimes smoothed out, while other disturbances starting as perfectly continuous motions cannot be maintained without generating discontinuities if the viscosity, resistivity, and the heat conduction of the fluid are negligible. Shock transitions occur only in a narrow region where the gradients of the flow velocity, the thermal pressure, and the magnetic field become very large while, outside of the transition region, the flows obey the laws established for smooth motions.

The discontinuities in MHD can be described by the following jump conditions, which can be obtained by integrating the conservation laws Eqs. (2.1)–(2.7) across the discontinuities:

$$W[V] = -[u_x], \tag{3.1}$$

$$W[u_x] = [P], \tag{3.2}$$

$$W[u_y] = [A_y], \tag{3.3}$$

$$W[u_z] = [A_z], \tag{3.4}$$

$$W[VB_y] = -B_x[u_y], \tag{3.5}$$

$$W[VB_z] = -B_x[u_z], \tag{3.6}$$

$$W[E] = [u_x P] + [u_y A_y] + [u_z A_z]. \tag{3.7}$$

Here W is the speed of the discontinuity surface propagating in the mass coordinate. In fact, it is the mass flux entering the surface. The bracket $[X]$ stands for the difference between the states on the two sides of the surface, i.e., $[X] = X_1 - X_0$. The speed W is negative when the discontinuity propagates in the negative m direction. In the remainder of this paper, the subscript "0" is referred to the evaluation at a pre-shock state unless it is specified otherwise. The post-shock state is denoted by the subscript "1." We mention that this set of jump conditions derived from the conservation laws in the Lagrangian coordinate is equivalent to those derived from the Eulerian equations in the book by Landau and Lifshitz [23].

Although the differential equations are meaningful only when flows are smooth, the integral form Eqs. (3.1)–(3.7) of the conservation laws holds even when the changes occur discontinuously in the form of jumps. The reason is that the conservation of mass, momentum, energy, and magnetic flux are more fundamental than the differential equations. This set of jump conditions can be derived from these conservation laws directly. The mass, momentum, energy, and magnetic flux are still conserved when the small dissipation terms neglected in Eqs. (2) are included. Since the conservation of these quantities implies that the jumps across shocks do not depend upon their internal structure, we may in fact obtain the viscosity, heat conduction, and resistivity which determine that internal structure. We will therefore suppose that the flows are completely determined by these jump conditions and that the specific entropy increases when the fluid crosses a shock, since the viscosity, heat conduction, and resistivity are neglected. In our Riemann solver, we will approximate rarefactions by rarefaction shocks obeying the jump conditions given above (and involving decreases in the entropy). This approximation limits the applicability of this work to weak rarefactions.

In the case of degenerate wave speeds, which occurs infrequently, Brio and Wu [16] have pointed out that the Riemann problem solution may depend upon the ratio of the small neglected terms in our conservation laws, and hence upon the internal structure of a wave which here is assumed to be discontinuous. We will ignore this complication here because our Riemann solver is intended mainly for use in the calculation of the time-averaged fluxes at the interfaces of numerical zones. If such degeneracies are important in a given numerical simulation, it must be the responsibility of the programmer to add appropriate physical and/or numerical dissipation terms to his or her computer code so that an appropriate ratio of different kinds of dissipation is obtained.

Since our Riemann solver deals with waves as discontinuities, we will first review five kinds of discontinuities in ideal MHD: contact discontinuities, tangential discontinuities, fast shocks, slow shocks, and rotational discontinuities. More detailed description of MHD discontinuities may be found in many standard texts (for example, Landau and Lifshits [23], Jeffrey and Taniuti [26], Kulikovskiy and Lyubimov [27], Kantrowitz and Petschek [28]). Contact discontinuities are associated with the characteristic of zero speed. No jump is allowed except in the density and energy in a contact discontinuity. A contact surface in MHD is one separating two parts of the fluid without any flow of the fluid through or along the surface. A tangential discontinuity can occur in the special case when the longitudinal component of the magnetic field vanishes and the density and the transverse components of both the magnetic field and the flow velocity jump discontinuously, but total pressure P and the longitudinal component of the flow velocity are continuous. Both contact and tangential discontinuities do not propagate in the Lagrangian coordinate, but there are jumps in the tangential components of the magnetic field and the flow velocity in a tangential discontinuity. The tangential discontinuity can be viewed as a limiting case in which the contact discontinuity, slow wave, and Alfven wave all tend to collapse into a single discontinuity as B_x tends to zero.

Shock fronts are discontinuity surfaces which are crossed by the fluid. The side of the shock front through which the fluid enters will be called the pre-shock state, the other, the post-shock state. There exist jumps in all the variables, including the density, the flow velocity, the pressure, and the magnetic field.

For a fast shock, the magnitude of each transverse component of the magnetic field is larger in its post-shock state and smaller in its pre-shock state. The increase of the magnitude from the pre-shock state to the post-shock state for a fast shock is due to both the compression and the shearing of the fluid. This is illustrated in Fig. 5a, where a fluid element is shown as it is in the pre-shock state and in the post-shock state for a fast shock. The fluid is sheared against the direction of the transverse component of the magnetic field in the post-shocks state for a fast shock. Thus

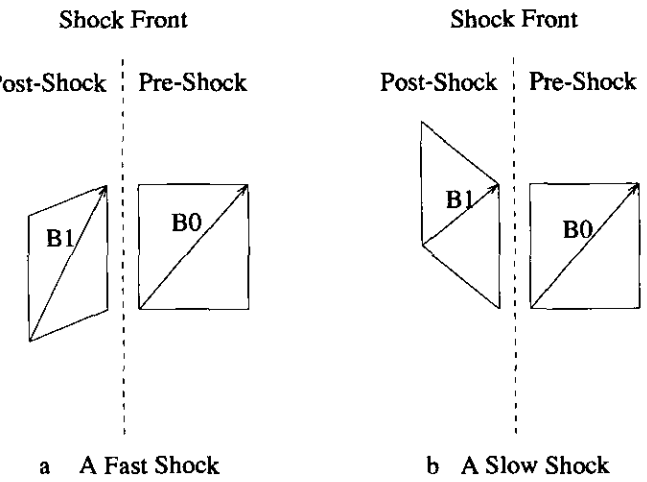

FIG. 5. The compressing and shearing for a MHD fast shock (a) and for a MHD slow shock (b). The fluid is sheared against the direction of the transverse component of the magnetic field for a fast shock and is sheared in the direction of the transverse component for slow shock.

the shearing makes the magnitudes of both transverse components of the magnetic field increase.

Across a slow shock, the magnitude of each transverse component of the magnetic field decreases from its pre-shock state to its post-shock state. This decrease results from the composition between the compression and the shearing of the fluid. The compression makes the magnitude of the transverse component of the magnetic field increase, while the shearing causes it to decrease because the fluid is sheared in the direction of the transverse component of the magnetic field in the post-shock state for a slow shock. Figure 5b shows a fluid element in the two sides of a slow shock front.

A rotational discontinuity propagates at the speed C_x. Across the discontinuity surface, the transverse part of the magnetic field undergoes a rotation around the normal of the surface, and its magnitude is unchanged. There are jumps in the transverse components of the flow velocity, but no jumps in the density, the thermal pressure, and the longitudinal component of the flow velocity. Thus the characteristic speeds on both sides of the surface are the same. For this reason, a rotational discontinuity cannot be formed by the steepening of a smooth disturbance. We mention that in the coordinate system moving with the velocity $\mathbf{v}_0$ ($\equiv \mathbf{B}_{t0}/\sqrt{4\pi\rho} + \mathbf{u}_{t0}$), where the subscript t denotes the transverse component, the flow velocity is rotated in the same way as the magnetic field, and its magnitude and angle to the normal remain unchanged in this moving coordinate system.

Switch-off shocks and switch-on shocks are two limiting cases for the slow and fast shocks, respectively. From the jump conditions, Eqs. (3.1)–(3.7), it is not difficult to see that there are two solutions for discontinuities which propagate at the speed W equal to C_{x0}, namely rotational discontinuities and switch-off shocks. For a switch-off shock, the tangential part of the magnetic field is non-zero in the pre-shock state but vanishes in the post-shock state. If a fast shock propagates along the magnetic field, i.e., the transverse part of the magnetic field in the pre-shock state is zero, if the magnetic field B_x is sufficiently large and if the shock speed W is precisely equal to C_{x1}, there will be a tangential component of the magnetic field behind the shock even though this component vanishes ahead of the shock. Such a shock is called a switch-on shock.

The above is a complete list of the possible discontinuities in ideal MHD. For the case where viscosity and resistivity are non-vanishing, Wu [14, 15, 20] has discussed phenomena of intermediate shocks. These phenomena will not concern us here, because our Riemann solver is designed for use in numerical simulations of ideal MHD. Simulations of more complete MHD equations can be constructed by adding dissipation terms as a separate numerical step, without altering the Riemann solver presented here.

Except switch-on and switch-off shocks, fast and slow shocks have the relations between their pre-shock state and post-shock state:

$$B_{z0}[B_y] = B_{y0}[B_z], \tag{4a}$$

$$B_{z0}[u_y] = B_{y0}[u_z]. \tag{5}$$

Thus across both fast and slow shocks, the transverse components of the magnetic field obey the relation:

$$\frac{B_{z1}}{B_{y1}} = \frac{B_{z0}}{B_{y0}}; \tag{4b}$$

i.e., the orientations of the transverse part of the magnetic field in the pre-shock states and the post-shock states are either exactly the same or opposite. The post-shock states for different shock speeds for a given pre-shock state are shown in Fig. 6, where both transverse components of the magnetic field keep the same sign in their pre-shock states and post-shock states. Thus the orientations of the transverse part of the magnetic field in post-shock states are exactly the same as those in pre-shock states for both fast and slow shocks except for switch-on and switch-off shocks.

If the thermal pressure, the magnetic field, the density in the pre-shock state (or in the post-shock state), and the shock speed are given, the jumps in all the variables can be found through the following cubic equation (e.g., in terms of the y-component of the magnetic field) and the general jump conditions:

$$\lambda[B_y]^3 + A_2[B_y]^2 + A_1[B_y] + A_0 = 0. \tag{6}$$

Here the coefficients are defined as

$$\lambda \equiv 1 + \left(\frac{B_z}{B_y}\right)^2,$$

$$A_2 \equiv \frac{1}{C_x^2}\lambda B_y((\gamma+2)\,C_x^2 - (\gamma-2)\,W^2),$$

$$A_1 \equiv \frac{4\pi V}{C_x^2}\{(\gamma+1)(W^2-C_x^2)^2 + \lambda C_y^2((\gamma+1)\,C_x^2 + (2-\gamma)\,W^2) - 2(W^2-C_f^2)(W^2-C_s^2)\},$$

$$A_0 \equiv -\frac{8\pi V}{C_x^2} B_y(W^2-C_f^2)(W^2-C_s^2).$$

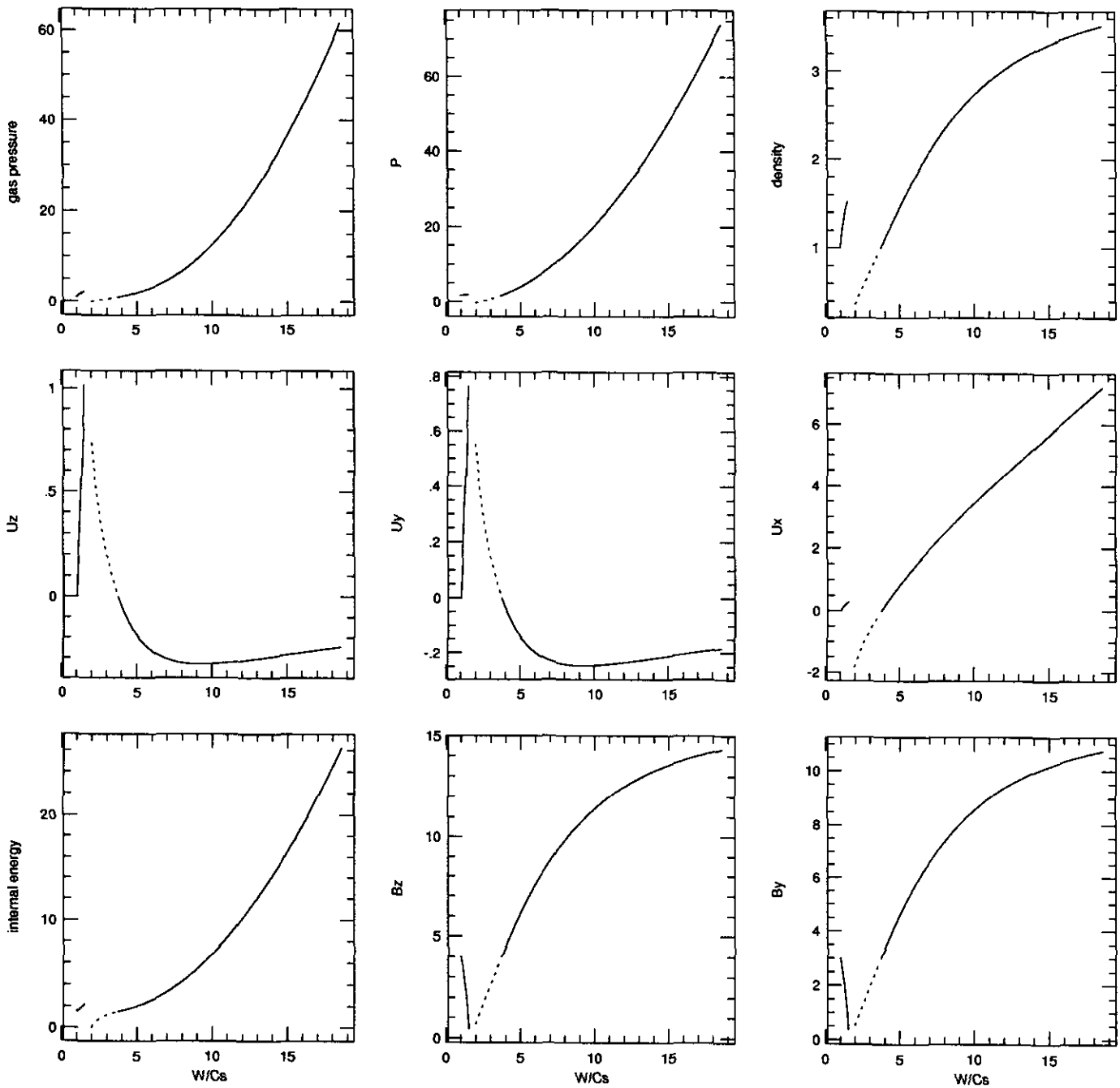

FIG. 6. The solutions of the MHD jump conditions for a given pre-shock state $(\rho, p, u_x, u_y, u_z, B_y, B_z) = (1, 1, 0, 0, 0, 3, 4)$ and different shock speeds W. Here $B_x = 3$ and $\gamma = \frac{5}{3}$. C_s is the MHD slow wave speed for the given pre-shock state. The dashed lines are for fast rarefaction waves computed from the jump conditions, the solid lines to the right of the dashed lines are for MHD fast shocks and the solid lines to the left are for the MHD slow shocks.

All the variables in the coefficients $\hat{\lambda}$, A_0, A_1, and A_2 are evaluated at the pre-shock state. The appropriate root for Eq. (6) should be chosen by the entropy condition. If more than one possible post-shock state is found, we evaluate the entropy for each possible post-shock state. The physical post-shock state must have larger entropy than that in the pre-shock state if the wave involves a compression.

An immediate result of Eq. (6) is the jump in the component B_y for the limiting case with $W \to \infty$, i.e., the largest possible jump across a shock

$$[B_y] = \frac{2}{(\gamma - 1)} B_{y0} \quad \text{when} \quad W \to \infty. \tag{7a}$$

Here the subscript "0" is used to refer to the pre-shock state. This formula is also valid for the z-component of the magnetic field. Using the general jump conditions, Eqs. (3.1)–(3.7), with this result, we find that the largest possible jump in the specific volume is the same as that in hydrodynamics:

$$[V] = -\frac{2}{(\gamma + 1)} V_0 \quad \text{when} \quad W \to \infty. \tag{7b}$$

These largest possible jumps are valid even for the special case with a vanishing longitudinal component of the magnetic field, which can be verified easily using Eq. (8) below and the general jump conditions.

A typical behavior for the dependence of the post-shock state on the shock speed W is given in Fig. 6, where the pre-shock state $(\rho, p, B_y, B_z) = (1, 1, 3, 4)$ with $B_x = 3$ and vanishing flow velocity, and the shock speed is normalized by the slow wave speed at the pre-shock state. The dashed lines correspond to fast rarefaction waves, the solid lines to the left of the dashed lines are for slow shocks, and the solid line to the right of the dashed lines are for fast shocks. The dividing line between slow shocks and fast rarefactions is $W/C_{x0} = 1$ and that between fast rarefactions and fast shocks $W/C_{f0} = 1$. It is easy to see that the post-shock state changes very rapidly with the slow shock speed. We point out again that we use the jump conditions to approximate rarefactions.

It is clear from the relation Eq. (4b) that both transverse components of the magnetic field at one side of a shock cannot vanish while they are not all zero at the other side, except for switch-on and swith-off shocks. For this reason we can separate the special case with uniformly vanishing

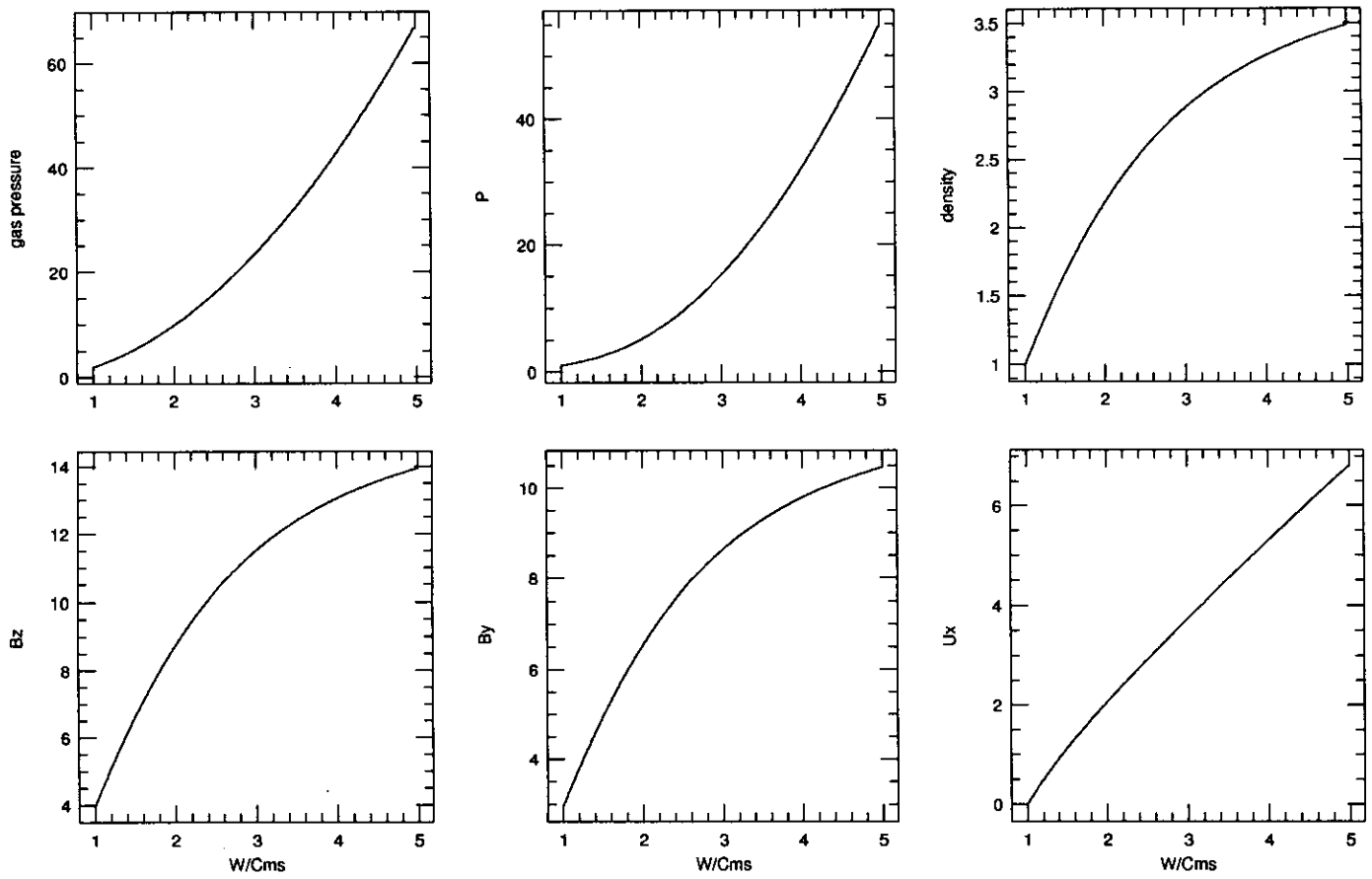

FIG. 7. The solutions of the MHD jump conditions for a given pre-shock state $(\rho, p, u_x, u_y, u_z, B_y, B_z) = (1, 1, 0, 0, 0, 3, 4)$ and for different shock speeds W in the case $B_x = 0$. Here C_{ms} is the magnetosonic wave speed for the given pre-shock state.

transverse components of the magnetic field from the general one discussed above. The dynamics in this special case is exactly the same as that in hydrodynamics, since the longitudinal component of the magnetic field plays no role in the dynamics if there are no transverse components of the magnetic field.

For the other special case with vanishing longitudinal component B_x of the magnetic field, magnetosonic shocks can occur. For magnetosonic shocks, we have the following relation between the pre-shock state, the jump in the total pressure P, and the shock speed W, which is equivalent to Eq. (6):

$$[P]=\frac{V}{2(\gamma+1)}(Q_1-\sqrt{Q_1^2-Q_2}),$$
$$Q_1\equiv(\gamma+3)\,W^2-2\gamma\rho P, \tag{8}$$
$$Q_2\equiv 8(\gamma+1)\,W^2(W^2-C_{\rm ms}^2).$$

Typical solutions for this relation and the jump conditions in the special case are shown in Fig. 7, where the pre-shocks state is the same as that in Fig. 6, except for the vanishing of B_x. There are no jumps in the transverse components of the flow velocity.

5. A NONLINEAR RIEMANN SOLVER

In general, given a left state and a right state, there are seven discontinuities which emanate from the original jump in our approximate treatment of the Riemann problem. The seven possible discontinuities separate the whole $(m-t)$ or $(x-t)$ space into eight possibly different regions. We will develop a Riemann solver here which can be used to determine the states in each of the eight regions from the given left and right states. Referring to Fig. 4 we will call the orientations of the transverse components of the magnetic field in regions R3 and R6, ψ_3 and ψ_6, respectively, i.e.,

$$\frac{B_{z3}}{B_{y3}}=\tan\psi_3,$$
$$\frac{B_{z6}}{B_{y6}}=\tan\psi_6.$$

From Eq. (4b) and the requirements for the contact discontinuity between the regions R4 and R5, we immediately obtain the following relation between the two orientations:

$$\tan\psi_3=\tan\psi_6.$$

Thus, the orientations in regions R3, R4, R5, and R6 must be the same. We call this common field orientation angle ψ. The orientations of the transverse components of the magnetic field in regions R2 and R7 may be different from ψ and different from each other. According to Eq. (4b), the orientations ψ_2 and ψ_7 in regions R2 and R7 are equal to those in the left state and right state, $\psi_{\rm L}$ and $\psi_{\rm R}$, respectively. If the orientations $\psi_{\rm L}$, $\psi_{\rm R}$, and ψ are the same, there can be no rotational discontinuity involved in this Riemann problem.

$$W_{\rm f,s}^2=\frac{1}{2(1+S_0)}\{(C_{\rm s}^2+C_{\rm f}^2+S_1)$$
$$\pm\sqrt{(C_{\rm s}^2+C_{\rm f}^2+S_1)^2-4(1+S_0)(C_{\rm s}^2C_{\rm f}^2-S_2)}\}. \tag{9}$$

Here the plus sign is for fast shocks and the minus sign for slow shocks. The coefficients S_0, S_1, and S_2 are defined as

$$S_0\equiv-\frac{1}{2}(\gamma-1)\frac{[A_y]}{A_y},$$
$$S_1\equiv\frac{1}{2}\left\{(\gamma-2)\,\lambda\rho\frac{B_y}{B_x}[A_y]+2C_0^2\right.$$
$$\left.-(\gamma-4)\,\lambda C_y^2-2\gamma C_x^2\right\}\frac{[A_y]}{A_y},$$
$$S_2\equiv\frac{1}{2}\{\lambda\rho^2[A_y]^2+(\gamma+2)\,\lambda\rho^2A_y[A_y]+\lambda(\gamma+1)\,C_x^2C_y^2$$
$$+(\gamma+1)\,C_x^4-2C_0^2C_x^2\}\frac{[A_y]}{A_y}.$$

All the variables in the coefficients are referred to pre-shock states except for the jump $[A_y]$.

For the special case with a vanishing longitudinal part of the magnetic field, we find an equivalent formula for magnetosonic shocks,

$$W^2=\tfrac{1}{2}((C_{\rm ms}^2+G_1)+\sqrt{(C_{\rm ms}^2+G_1)^2-G_2}). \tag{10}$$

Here G_1 and G_2 are defined as

$$G_1\equiv\tfrac{1}{2}(\gamma+3)\,\rho[P],$$
$$G_2\equiv 2\rho^2\{(\gamma+1)[P]+2\gamma P\}[P].$$

Equations (9) and (10) are nonlinear. We note that a formula similar to Eq. (9) can be obtained by replacement of the y component by the z component if the y component of the magnetic field vanishes.

For any given left and right states, we construct the Riemann solution by the following procedures:

(1) Guess one transverse component (e.g., y-component) B_{y2}, B_{y4}, and B_{y7} of the magnetic field in regions R2, R4, and R7, and the common orientation of the transverse part of the magnetic field in regions R3, R4, R5, and R6, ψ. Here $\tan\psi=B_{z3}/B_{y3}$.

(2) Consider the right state and the left state as two pre-shock states; calculate two fast shock speeds, one for the wave moving to the right, the other for the wave moving to the left; then apply the jump conditions Eqs. (3.1)–(3.7) with these two fast shock speeds and the magnetic field component B_y in the two post-shock states to obtain the complete states in regions R2 and R7, respectively.

(3) Perform the rotations with the earlier guess ψ; then use the jump conditions Eqs. (3.1)–(3.7) with the speed W equal to the Alfven speeds in regions R3 and R6 to obtain the states in regions R3 and R6, respectively.

(4) Consider the states in regions R3 and R6 as two pre-shock states, repeat the procedure (2) for two slow shocks instead of the fast shocks to obtain the states in regions R4 and R5.

(5) Apply the conditions for a contact discontinuity between regions R4 and R5 to improve the earlier guess on B_{y2}, B_{y4}, B_{y7}, and ψ, as described below. With this improved guess, go back to procedure (1).

Following the first four steps, the state in region R4 is a function of the transverse components of the magnetic field in regions R2 and R4, and the orientation ψ, and the state in region R5 is a function of the transverse components of the magnetic field in the regions R7 and R4, and the orientation ψ. If B_{y2}, B_{y4}, B_{y7}, and the orientation ψ are the solutions of the Riemann problem, the two states in regions R4 and R5 should be the same except for their densities and energies, i.e.,

$$
\begin{aligned}
u_{x4}(B_{y2}, B_{y4}, \psi) &= u_{x5}(B_{y7}, B_{y4}, \psi),\\
u_{y4}(B_{y2}, B_{y4}, \psi) &= u_{y5}(B_{y7}, B_{y4}, \psi),\\
u_{z4}(B_{y2}, B_{y4}, \psi) &= u_{z5}(B_{y7}, B_{y4}, \psi),\\
p_4(B_{y2}, B_{y4}, \psi) &= p_5(B_{y7}, B_{y4}, \psi).
\end{aligned}
$$

This set of equations can be solved for B_{y2}, B_{y4}, B_{y7}, and ψ iteratively by Newton's method; i.e., we have the following equations for the modifications δB_{y2}, δB_{y4}, δB_{y7}, and $\delta\psi$ for the initial guess on B_{y2}, B_{y4}, B_{y7}, and ψ:

$$
\frac{\partial u_{x4}}{\partial B_{y2}}\delta B_{y2}+\left(\frac{\partial u_{x4}}{\partial B_{y4}}-\frac{\partial u_{x5}}{\partial B_{y4}}\right)\delta B_{y4}-\frac{\partial u_{x5}}{\partial B_{y7}}\delta B_{y7}+\left(\frac{\partial u_{x4}}{\partial\psi}-\frac{\partial u_{x5}}{\partial\psi}\right)\delta\psi=u_{x5}-u_{x4}, \tag{11a}
$$

$$
\frac{\partial u_{y4}}{\partial B_{y2}}\delta B_{y2}+\left(\frac{\partial u_{y4}}{\partial B_{y4}}-\frac{\partial u_{y5}}{\partial B_{y4}}\right)\delta B_{y4}-\frac{\partial u_{y5}}{\partial B_{y7}}\delta B_{y7}+\left(\frac{\partial u_{y4}}{\partial\psi}-\frac{\partial u_{y5}}{\partial\psi}\right)\delta\psi=u_{y5}-u_{y4}, \tag{11b}
$$

$$
\frac{\partial u_{z4}}{\partial B_{y2}}\delta B_{y2}+\left(\frac{\partial u_{z4}}{\partial B_{y4}}-\frac{\partial u_{z5}}{\partial B_{y4}}\right)\delta B_{y4}-\frac{\partial u_{z5}}{\partial B_{y7}}\delta B_{y7}+\left(\frac{\partial u_{z4}}{\partial\psi}-\frac{\partial u_{z5}}{\partial\psi}\right)\delta\psi=u_{z5}-u_{z4}, \tag{11c}
$$

$$
\frac{\partial p_4}{\partial B_{y2}}\delta B_{y2}+\left(\frac{\partial p_4}{\partial B_{y4}}-\frac{\partial p_5}{\partial B_{y4}}\right)\delta B_{y4}-\frac{\partial p_5}{\partial B_{y7}}\delta B_{y7}+\left(\frac{\partial p_4}{\partial\psi}-\frac{\partial p_5}{\partial\psi}\right)\delta\psi=p_5-p_4. \tag{11d}
$$

It is quite tedious to write any derivative in the Jacobian in one formula. Let us consider one derivative of u_{x5} as an example. When we obtain u_{y5} in the fourth step in the MHD Riemann solver described above, u_{y5} is a function of the slow shock speed W_s and the state in R6, i.e.,

$$
\begin{aligned}
u_{y5} &= u_{y6}-\frac{B_x}{4\pi W_s}(B_{y5}-B_{y6}).\\
V_5 &= V_6-\frac{1}{B_{y5}}\left[B_x(u_{y5}-u_{y6})\frac{1}{W_s}+V_6(B_{y5}-B_{y6})\right].\\
u_{x5} &= u_{x6}-W_s(V_5-V_6).
\end{aligned}
$$

Thus u_{x5} is a function of W_s, V_6, B_{y5}, and B_{y6}. According to Eq. (9), the slow shock speed W_s is a function B_{y5} and the state in R6, i.e.,

$$
W_s = W_s(B_{y5}, \rho_6, p_6, B_{y6}, B_{z6}).
$$

The state in R6 is dependent upon the state in R7 and the orientation ψ, i.e.,

$$
\begin{aligned}
&V_6 = V_7, \qquad p_6 = p_7, \qquad u_{x6} = u_{x7},\\
&B_{y6} = \cos\psi\sqrt{B_{y7}^2+B_{z7}^2},\\
&B_{z6} = \sin\psi\sqrt{B_{y7}^2+B_{z7}^2},\\
&u_{y6} = u_{y7}-\frac{B_x}{4\pi C_{x7}}(B_{y6}-B_{y7}),\\
&u_{z6} = u_{z7}-\frac{B_x}{4\pi C_{x7}}(B_{z6}-B_{z7}).
\end{aligned}
$$

The state in R7 depends on the fast shock speed W_f and B_{y7}, where the fast shock speed W_f is a function of B_{y7} according to Eq. (9).

Since the dependence of u_{x5} on B_{y7} involves a lot of nested functions, we did not write down the derivative $\partial u_{x5}/\partial B_{y7}$ in one formula in our calculation. We find the derivative $\partial u_{x5}/\partial B_{y7}$ in the way for nested functions.

We point out that if the y-component of the magnetic field vanishes in some regions, e.g., in regions R1 or R3, we should use the formula in Eq. (9) with the replacement of

the y component by the z component. If the transverse part of the magnetic field in the left (or right) state does not vanish, that part in region R2 (or R7) cannot be zero either, as shown in Fig. 5 for fast shocks. The left and right states such that the transverse part of the magnetic field vanishes in one state, but not in the other, satisfy the jump conditions only when a switch-on or switch-off shock is involved.

For the special case without the longitudinal component of the magnetic field, the possible discontinuities separate all $(m-t)$ or $(x-t)$ space into only four possibly different regions. Referring to Fig. 2, fast shocks will be replaced by magnetosonic shocks. The states in regions R2, R3, and R4 are the same and the regions R5, R6, and R7 have another common state. The densities, the transverse components of the flow velocities, and the magnetic fields in the regions R4 and R5 may be different if there is a tangential discontinuity involved.

For these special cases, following the method used in PPM for the hydrodynamic case, we construct the Riemann solver as follows. We first guess the common total pressure P in the regions R4 and R5 instead of the magnetic field. Then considering the left and right states as two pre-shock states and using Eq. (10), we calculate the two possible magnetosonic shock speeds, one for the wave moving to the left and the other for the wave moving to the right. After this, we apply jump conditions with these two shock speeds to obtain the complete states in the regions R4 and R5, respectively. Finally the condition for a tangential discontinuity between the regions R4 and R5 is used to improve the initial guess on the common total pressure in the regions R4 and R5. The condition for a tangential discontinuity is that the longitudinal flow velocity must be the same in the regions R4 and R5 as well as their total pressures. With this improved total pressure replacing the initial guess, we go back to the first step for the iteration. The necessary formulae for this procedure follows:

$$u_{x4}(P_4, W_-(P_4)) = u_{x5}(P_4, W_+(P_4)),$$

$$\left(\frac{\partial u_{x4}}{\partial P_4} + \frac{\partial u_{x4}}{\partial W_-}\frac{\partial W_-}{\partial P_4} - \frac{\partial u_{x5}}{\partial P_4} - \frac{\partial u_{x5}}{\partial W_+}\frac{\partial W_+}{\partial P_4}\right)\delta P_4 = u_{x5} - u_{x4}.$$

Here the shock speeds $W_\pm$ are the positive shock speed and the negative shock speed calculated according to Eq. (10).

In the general case, an appropriate initial guess is very critical in this Riemann solver for strong discontinuities. If the initial guess makes the term in the square root of Eq. (9) negative, or if it makes $W_{f,s}^2$ negative, the iterations cannot be carried our further. Although several ways to find an appropriate initial guess have been tried, it is still difficult to find a method which works for all left and right states. The first way we have investigated is that the initial guess is calculated by the linear Riemann solver developed earlier. For weak discontinuities and some strong discontinuities, the initial guess from the linear Riemann solver works quite well, but it does not work for some of Riemann problems involving strong discontinuities.

Another investigation for the initial guess is to choose B_{y2}, B_{y4}, B_{y7}, and ψ simply as B_{yL} or B_{yR} and $\tan^{-1}(B_{zL}/B_{yL})$ or $\tan^{-1}(B_{zR}/B_{yR})$, appropriately. The most frequently occurring left and right states in numerical MHD simulations involve only one strong discontinuity and some other weak discontinuities. Thus, for the purpose of the initial guess, we assume that the Riemann problem involves only one strong discontinuity and some other weak discontinuities. We may estimate the kind of the strong discontinuity and the direction of its propagation in some way. If the strong discontinuity is a slow shock propagating to the right, we simply guess $B_{y7} = B_{yR}$, $B_{y4} = B_{y2} = B_{yL}$, and $\psi = \tan^{-1}(B_{yL}/B_{zL})$. We prefer to use the second method rather than the first to find the initial guess for strong discontinuities. In numerical computations, to assure that the assumption of a single strong wave (or no strong wave) is justified, it may be necessary to orient the x-direction used here to be orthogonal to this strong wave front before the Riemann solver is applied.

It is often desired to unify the two approaches for the initial guess, one of which works for weak discontinuities and the other which works for strong discontinuities. As we know, characteristics converge to a shock from both sides of a shock if there exists a shock. The Riemann invariants from each family are different between the two sides of a shock front. The more different the Riemann invariants between the left and right states are the stronger is the shock. Thus we can choose the difference of Riemann invariants of each family between left and right states to estimate the strength of the discontinuities involved in a particular MHD Riemann problem. We may define a weighting factor according to the difference in the Riemann invariants of the same family. Finally we use the weighting factor to average two initial guesses from the linear Riemann solver and from the appropriate choice between left and right states. In order to use the difference of the Riemann invariants to estimate the strength of discontinuities, more appropriate Riemann invariants for this purpose are $dR_{f\pm}$, defined in the third section, divided by $(C_f^2 - C_x^2)$, $dR_{s\pm}$ divided by $(C_s^2 - C_x^2)$, and $R_{a\pm}$ divided by $B_x \max(|B_y|, |B_z|)^2/4\pi$, respectively. The largest absolute value among the differences of these new Riemann invariants between left and right states, which is multiplied by a quarter, is found to be an appropriate weighting factor. If it is larger than unity, we set it to be unity in our program. All the examples given below are solved using the initial guess from this averaging procedure.

If there are several strong discontinuities generated from left and right states, it is possible for an improved guess to be far from both the initial guess and the final solution. This will possibly make the iteration stop because of the terrible

guess. In order to make the iteration gradually converge to the final solution, we put a relaxation factor in the Newton iteration Eqs. (11a)–(11d) for multiple strong discontinuities; i.e., we multiply the right sides of Eqs. (11a)–(11d) by a factor $(1-f^N)$, where f is a positive number less than one and N is the number of iterations carried out. The fourth example below is solved by this relaxation method. In MHD simulations, the actual value of f can be chosen according to the difference of left and right states. For a larger difference, f is chosen to be larger.

We should point out that for some left and right states, this relaxation still does not work. We give an example for such cases. Since we use the Riemann solver only for the calculation of time-averaged fluxes at the interfaces of numerical zones, we can still give some reasonable fluxes if the Riemann solver failed to find a solution for a specific Riemann problem. Reasonable results can still be reached in MHD simulations in this way even if the Riemann solver failed at a specific point in time and space.

Now we apply this Riemann solver to several typical examples. We set the specific heat $\gamma = \frac{5}{3}$ in all the examples unless they are specified otherwise. All the motions of waves in the following example are measured in the Lagrangian coordinate. The rotated angles $\delta\psi_L$ and $\delta\psi_R$ are defined as $\delta\psi_L = (\psi_3 - \psi_2)$ and $\delta\psi_R = (\psi_6 - \psi_7)$, respectively. For those MHD Riemann problems which involve no rarefaction waves, our Riemann solver is exact.

We first give an MHD Riemann problem which involves multiple weak discontinuities. The left and right states for this example are $(\rho, p, u_x, u_y, u_z, B_y, B_z)_L = (1.08, 0.95, 1.2, 0.01, 0.5, 3.6, 2.0)$ and $(\rho, p, u_x, u_y, u_z, B_y, B_z)_R = (1.0, 1.0, 0.0, 0.0, 0.0, 4.0, 2.0)$ with B_x being two. This Riemann problem involves two fast shocks with their Mach numbers 1.22 and 1.28, respectively, two slow shocks of Mach numbers, 1.09 and 1.07, two rotational discontinuities with their rotated angles 12° and 9°, respectively, and one contact discontinuity. Table Ia shows the solutions for the states in each region, and Table Ib contains the results for the shock speeds and rotated angles from each iteration.

The second example is about magnetosonic shocks. The left and right states in this example are $(\rho, p, u_x, B_y, B_z)_L = (0.1, 0.4, 50, -1, -2)$ and $(\rho, p, u_x, B_y, B_z)_R = (0.1, 0.2, 0, 1, 2)$ with vanishing transverse components of the flow velocity. This single discontinuity will generate two strong magnetosonic shocks, one moving to the right with its Mach number 12.4 and the other moving to the left with its Mach number 10.3. Table IIa gives the solutions of the Riemann problem in different regions. The states in regions R2 and R3 are the same as that in region R4 and the states in regions R6 and R7 are the same as that in region R5. Both transverse components of the flow velocity are the same for all regions. Both transverse components of the magnetic field increase across both shocks from the pre-shock state to the post-shock state. Table IIb shows the convergence of the shock speeds.

The third example we will show that the Riemann problem involves no rotational discontinuities. The left and right states are chosen as $(\rho, p, B_y)_L = (1, 1, 5)$,

TABLE Ia

A Riemann Problem and Its Solutions

Regions	ρ	p	u_x	u_y	u_z	B_y	B_z
R1	1.0800E+00	9.5000E−01	1.2000E+00	1.0000E−02	5.0000E−01	3.6000E+00	2.0000E+00
R2	1.4903E+00	1.6558E+00	6.0588E−01	1.1235E−01	5.5686E−01	5.0987E+00	2.8326E+00
R3	1.4903E+00	1.6558E+00	6.0588E−01	2.2157E−01	3.0125E−01	5.5713E+00	1.7264E+00
R4	1.6343E+00	1.9317E+00	5.7538E−01	4.7601E−02	2.4734E−01	5.0074E+00	1.5517E+00
R5	1.4735E+00	1.9317E+00	5.7538E−01	4.7601E−02	2.4734E−01	5.0074E+00	1.5517E+00
R6	1.3090E+00	1.5844E+00	5.3432E−01	−1.8411E−01	1.7554E−01	5.7083E+00	1.7689E+00
R7	1.3090E+00	1.5844E+00	5.3432E−01	−9.4572E−02	−4.7286E−02	5.3452E+00	2.6726E+00
R8	1.0000E+00	1.0000E+00	0.0000E+00	0.0000E+00	0.0000E+00	4.0000E+00	2.0000E+00

TABLE Ib

The Sequence of Iterations for Shock Speeds

Iteration	W_{f-}	W_{s-}	W_{s+}	W_{f+}	$\delta\psi_1$	$\delta\psi_r$
0	−2.2996E+00	−5.2268E−01	4.7068E−01	2.1730E+00	−7.8971E+00	−5.4075E+00
1	−2.3286E+00	−5.1576E−01	4.8196E−01	2.2644E+00	−1.2020E+01	−9.5303E+00
2	−2.3305E+00	−5.1593E−01	4.8143E−01	2.2638E+00	−1.1837E+01	−9.3479E+00
3	−2.3305E+00	−5.1594E−01	4.8144E−01	2.2638E+00	−1.1838E+01	−9.3481E+00

Note. $B_x = 2.0$, $\gamma = \frac{5}{3}$.

TABLE IIa

A Riemann Problem and Its Solutions

Regions	ρ	p	u_x	B_y	B_z
R1	1.00000E−01	4.00009E−01	5.00000E+01	−1.00000E+00	−2.00000E+00
R4	3.87123E−01	8.16610E+01	2.50333E+01	−3.87123E+00	−7.74247E+00
R5	3.90431E−01	8.16098E+01	2.50333E+01	3.90431E+00	7.80862E+00
R8	1.00000E−01	2.00000E−01	0.00000E+00	1.00000E+00	2.00000E+00

TABLE IIb

The Sequence of Iterations for Shock Speeds

Iteration	W_{f-}	W_{f+}
0	−3.26279E−01	3.18465E−01
1	−1.12315E+00	1.12075E+00
2	−2.46048E+00	2.45921E+00
3	−3.23887E+00	3.23787E+00
4	−3.36376E+00	3.36280E−00
5	−3.36622E+00	3.36526E+00
6	−3.36622E+00	3.36526E+00

Note. $B_x = 0, \gamma = \frac{5}{3}$.

Table IIIa

A Riemann Problem and Its Solutions

Regions	ρ	p	u_x	u_y	u_z	B_y	B_z
R1	1.0000E+00	1.0000E+00	0.0000E+00	0.0000E+00	0.0000E+00	5.0000E+00	0.0000E+00
R2	1.9185E+00	3.6771E+00	1.6671E+00	3.5507E−01	0.0000E+00	1.0179E+00	0.0000E+00
R3	1.9185E+00	3.6771E+00	−1.6671E+00	3.5507E−01	0.0000E+00	1.0179E+01	0.0000E+00
R4	2.8546E+00	7.6459E+00	−1.8549E+00	−1.2024E+00	0.0000E+00	3.0094E+00	0.0000E+00
R5	8.5164E−02	7.6459E+00	−1.8549E+00	−1.2024E+00	0.0000E+00	3.0094E+00	0.0000E+00
R6	8.6858E−03	7.9015E+00	−1.7991E+00	5.5200E−02	0.0000E+00	1.7251E+00	0.0000E+00
R7	8.6858E−02	7.9015E+00	−1.7991E+00	5.5200E−02	0.0000E+00	1.7251E+00	0.0000E+00
R8	1.0000E−01	1.0000E+01	0.0000E+00	0.0000E+00	0.0000E+00	2.0000E+00	0.0000E+00

Table IIIb

The Sequence of Iterations for Wave Speeds and Rotated Angles

Iteration	W_{f-}	W_{s-}	W_{s+}	W_{f+}	$\delta\psi_l$	$\delta\psi_r$
0	−2.0198E+00	−7.6713E−01	2.6499E−01	1.3038E+00	0.0000E+00	0.0000E+00
1	−4.1821E+00	−1.1950E+00	2.3241E−01	1.1398E+00	0.0000E+00	0.0000E+00
2	−3.5886E+00	−1.1173E+00	2.4275E−01	1.1838E+00	0.0000E+00	0.0000E+00
3	−3.4851E+00	−1.0997E+00	2.4379E−01	1.1889E+00	0.0000E+00	0.0000E+00
4	−3.4822E+00	−1.0990E+00	2.4380E−01	1.1891E+00	0.0000E+00	0.0000E+00

Note. $B_x = 3.0, \gamma = \frac{5}{3}$.

$(\rho, p, B_y)_R = (0.1, 10, 2)$ with B_z and the flow velocity $\mathbf{u}$ equal to zero in the both states. The longitudinal field B_x is three in this example. The solution of this Riemann problem is given in Table IIIa. It contains one fast shock with Mach number $M_{f-} = 1.724$ and one slow shock with Mach number $M_{s-} = 1.457$ moving to the left, one fast rarefaction wave and one slow rarefaction wave moving to the right, and one contact discontinuity. The magnetic field component B_z and the flow velocity component u_z are zero in all the regions. Table IIIb shows the sequence of the iterations for the wave (either shock or rarefaction) speeds $W_{s\pm}$ and $W_{f\pm}$, where the numbers in the first row come from the initial guess, and the remaining one comes from each iteration.

The fourth example is specifically chosen for comparison with the results given by Brio and Wu [16]. We take $(\rho, p, B_y)_L = (1, 1, \sqrt{4\pi})$, $(\rho, p, B_y)_R = (0.125, 0.1, -\sqrt{4\pi})$, with B_x being 2.6587 and the vanishing flow velocity $\mathbf{u}$ and the field component B_z in both the left and right states; γ in this example is set to be two for the comparison of our result whith those in previous work. The single initial discontinuity will develop into two fast rarefaction waves propagating in opposite directions, two slow shocks, one of which propagates to the right at its Mach number 2.2 and the other of which propagates to the left at its Mach number 1.05, one rotational discontinuity with $-180°$ rotation and one contact discontinuity, as shown in Tables IVa and IVb.

We point out that this pair of left and right states is the same as that in the work done by Brio and Wu [16] and recent work done by Zachary and Colella [22], where a solution involving a compound wave is presented. According to the MHD jump conditions equations (3.1)–(3.7), the discontinuity which can change the sign of transverse components of the magnetic field is exclusively the rotational discontinuity for the case of non-vanishing B_x. It is interesting to consider the states in R2 and R7 in the example above as the left and right state of a new MHD Riemann problem. We note that the left and right states are the same as the two post-wave states for the two fast rarefaction waves in the work by Brio and Wu [16] and the work by Zachary and Colella [22]. According to our MHD Riemann solver, this Riemann problem will involve two slow shocks, one rotational discontinuity, and one contact discontinuity as in the example above. Since there is no longer any rarefaction wave involved, our Riemann solver is exact for this MHD Riemann problem. When we use these left and right states as an initial condition for a 1D MHD numerical simulation, we find the same wave pattern involving the compound wave as shown in [16, 22]. We will report our 1D MHD simulations in another paper in detail. Apparently, this Riemann problem does not have a unique solution.

Tables Va and Vb are for the Riemann problem: $(\rho, p, u_x, u_y, u_z, B_y, B_z)_L = (1.1, 5.6, 4, 0, 0, 5.0, -3.5)$ and $(\rho, p, u_x,$

Table IVa

A Riemann Problem and Its Solutions

Regions	ρ	p	u_x	u_y	u_z	B_y	B_z
R1	1.0000E+00	1.0000E+00	0.0000E+00	0.0000E+00	0.0000E+00	3.5449E+00	0.0000E−00
R2	6.8523E−01	4.4545E−01	6.3274E−01	−2.1509E−01	−6.0676E−01	2.1446E+00	6.0498E−09
R3	6.8523E−01	4.4545E−01	6.3274E−01	−1.6768E+00	−6.6560E−01	−2.1446E+00	−1.8749E−07
R4	7.3224E−01	5.0883E−01	5.8525E−01	−1.5749E+00	−5.7652E−08	−1.9004E+00	−1.6614E−07
R5	2.3451E−01	5.0883E−01	5.8525E−01	−1.5749E+00	1.1541E−07	−1.9004E+00	−1.6614E−07
R6	1.1665E−01	8.6904E−02	−2.5050E−01	−1.7430E−01	2.3786E−07	−3.1845E+00	−2.7840E−07
R7	1.1665E−01	8.6904E−02	−2.5050E−01	−1.7430E−01	4.9169E−10	−3.1845E+00	8.9834E−09
R8	1.2500E−01	1.0000E−01	0.0000E+00	0.0000E+00	0.0000E+00	−3.5449E+00	0.0000E−00

Table IVb

The Sequence of Iterations for Wave Speeds and Rotated Angles

Iteration	W_{f-}	W_{s-}	W_{s+}	W_{f+}	$\delta\psi_l$	$\delta\psi_r$
0	−1.5774E+00	−5.4093E−01	8.4216E−02	4.1600E−01	1.7992E+02	8.1566E−02
1	−1.3677E+00	−4.4824E−01	1.4373E−01	4.1763E−01	1.7992E+02	8.1566E−02
2	−1.3654E+00	−4.9123E−01	1.8494E−01	4.3134E−01	1.7992E+02	8.1566E−02
3	−1.3767E+00	−5.0627E−01	1.9365E−01	4.3718E−01	1.7992E+02	8.1566E−02
4	−1.3774E+00	−5.0696E−01	1.9398E−01	4.3745E−01	1.7992E+02	8.1566E−02
5	−1.3774E+00	−5.0696E−01	1.9398E−01	4.3745E−01	1.7992E+02	8.1566E-02

Note. $B_x = 2.6587$, $\gamma = 2$.

Table Va

A Riemann Problem and Its Solutions

Regions	ρ	p	u_x	u_y	u_z	B_y	B_z
R1	1.1000E+00	5.6000E+00	4.0000E+00	0.0000E+00	0.0000E+00	5.0000E+00	−3.5000E+00
R2	2.3369E+00	2.3753E+01	5.9437E−01	3.4841E−01	−2.4389E−01	1.1198E+01	−7.8383E+00
R3	2.3369E+00	2.3753E+01	5.9437E−01	7.8667E−01	9.0440E−01	1.3573E+01	−1.6156E+00
R4	2.5339E+00	2.7200E+01	5.2958E−01	7.6251E−02	9.8897E−01	1.0095E+01	−1.2017E+00
R5	3.4751E+00	2.7200E+01	5.2958E−01	7.6251E−02	9.8897E−01	1.0095E+01	−1.2017E+00
R6	3.0599E+00	2.1952E+01	4.4313E−01	−8.1869E−01	1.0955E+00	1.5074E+01	−1.7943E+00
R7	3.0599E+00	2.1952E+01	4.4313E−01	−5.7740E−01	−2.8870E−01	1.3578E+01	6.7889E+00
R8	1.0000E+00	1.0000E+00	−4.0000E+00	0.0000E+00	0.0000E+00	4.0000E+00	2.0000E+00

Table Vb

The Sequence of Iterations for Wave Speeds and Rotated Angles

Iteration	W_{f-}	W_{s-}	W_{s+}	W_{f+}	$\delta\psi_l$	$\delta\psi_r$
0	−3.3667E+00	−1.2090E+00	9.1163E−01	2.1461E+00	−3.0553E+02	−7.0885E+00
1	−5.7345E+00	−1.4637E+00	2.4161E+00	7.8614E+00	3.0425E+01	3.2887E+02
2	−7.2702E+00	−1.9679E+00	2.2096E+00	6.6764E+00	2.8082E+01	3.2653E+02
3	−7.0831E+00	−1.9484E+00	2.2135E+00	6.6004E+00	2.8195E+01	3.2664E+02
4	−7.0777E+00	−1.9476E+00	2.2136E+00	6.6001E+00	2.8204E+01	3.2665E+02
5	−7.0777E+00	−1.9476E+00	2.2136E+00	6.6001E+00	2.8204E+01	3.2665E+02

Note. $B_x = 5.0$, $\gamma = \frac{5}{3}$.

u_y, u_z, B_y, $B_z)_R = (1, 1, 0, 0, 0, 4, 2)$ with B_x being five. We have used the relaxation factor $f = 0.5$ in this example. Table Va shows the converged solution for the Riemann problem in all the regions. Table Vb displays the convergence process for shock speeds and rotated angles. The final row in Table Vb is the converged solution. It is clear that the solutions display two strong fast shocks with their Mach numbers $M_{f-} = 3.07$ and $M_{f+} = 5.133$, two slow shocks with $M_{s-} = 1.09$ and $M_{s+} = 1.07$, two rotations, and one contact discontinuity. Although the Mach numbers for the two slow shocks are small, the jumps of the magnetic field across the slow shocks are not small.

Finally we give an example in which the initial guess from the second method discussed before does not work. The left and right states are $(\rho, p, u_x, u_y, u_z, B_y, B_z)_L = (1, 20, 10, 0, 0, 5, 0)$, $(\rho, p, u_x, u_y, u_z, B_y, B_z)_R = (1, 1, -10, 0, 0, 5, 0)$ with B_x equal five. Table VI gives the solution of the Riemann problem in all the regions if an appropriate initial guess can be found. This Riemann problem contains two fast shocks with Mach numbers $M_{f+} = 6.54$ and $M_{f-} = 2.49$, one weak slow shock, one slow rarefaction, and one contact discontinuity. Since the MHD Riemann solver developed here is for the calculation of time-averaged fluxes at the interfaces of numerical zones in MHD simulations.

Table VI

A Riemann Problem and Its Solutions

Regions	ρ	p	u_x	u_y	u_z	B_y	B_z
R1	1.0000E+00	2.0000E+01	1.0000E+01	0.0000E+00	0.0000E+00	5.0000E+00	0.0000E+00
R2	2.6797E+00	1.5098E+02	7.2113E−01	2.3138E−01	0.0000E+00	1.3608E+01	0.0000E+00
R3	2.6797E+00	1.5098E+02	7.2113E−01	2.3138E−01	0.0000E+00	1.3608E+01	0.0000E+00
R4	2.6713E+00	1.5019E+02	7.2376E−01	3.5683E−01	0.0000E+00	1.4314E+01	0.0000E+00
R5	3.8508E+00	1.5019E+02	7.2376E−01	3.5683E−01	0.0000E+00	1.4314E+01	0.0000E+00
R6	3.7481E+00	1.4357E+02	7.0505E−01	−3.8803E−01	0.0000E+00	1.9239E+01	0.0000E+00
R7	3.7481E+00	1.4357E+02	7.0505E−01	−3.8803E−01	0.0000E+00	1.9239E+01	0.0000E+00
R8	1.0000E+00	1.0000E+00	−1.0000E+01	0.0000E+00	0.0000E+00	5.0000E+00	0.0000E+00

Note. $B_x = 5.0$, $\gamma = \frac{5}{3}$.

Any reasonable fluxes can be used if the Riemann solver failed at a specific interface and at a specific time. It should be noted that this example involves two very strong waves, a solution which arises only rarely during a numerical computation and which is invariably of a transient nature. The numerical computation recovers easily from such transients, as is illustrated below.

Figure 8 shows the results of MHD simulations with the initial condition $(\rho, p, u_x, u_y, u_z, B_y, B_z)_L = (1, 20, 10, 0, 0, 0, 5, 0)$ for $x < 0.5$ and $(\rho, p, u_x, u_y, u_z, B_y, B_z)_R = (1, 1, -10, 0, 0, 5, 0)$ for $x > 0.5$, where 200 uniform numerical zones are used. The dashed lines in Fig. 8 are the initial conditions, and the solid lines are the profiles of the physical variables after all the discontinuities generated from the initial single discontinuity are separated. The initial guess failed for these left and right states and the MHD Riemann

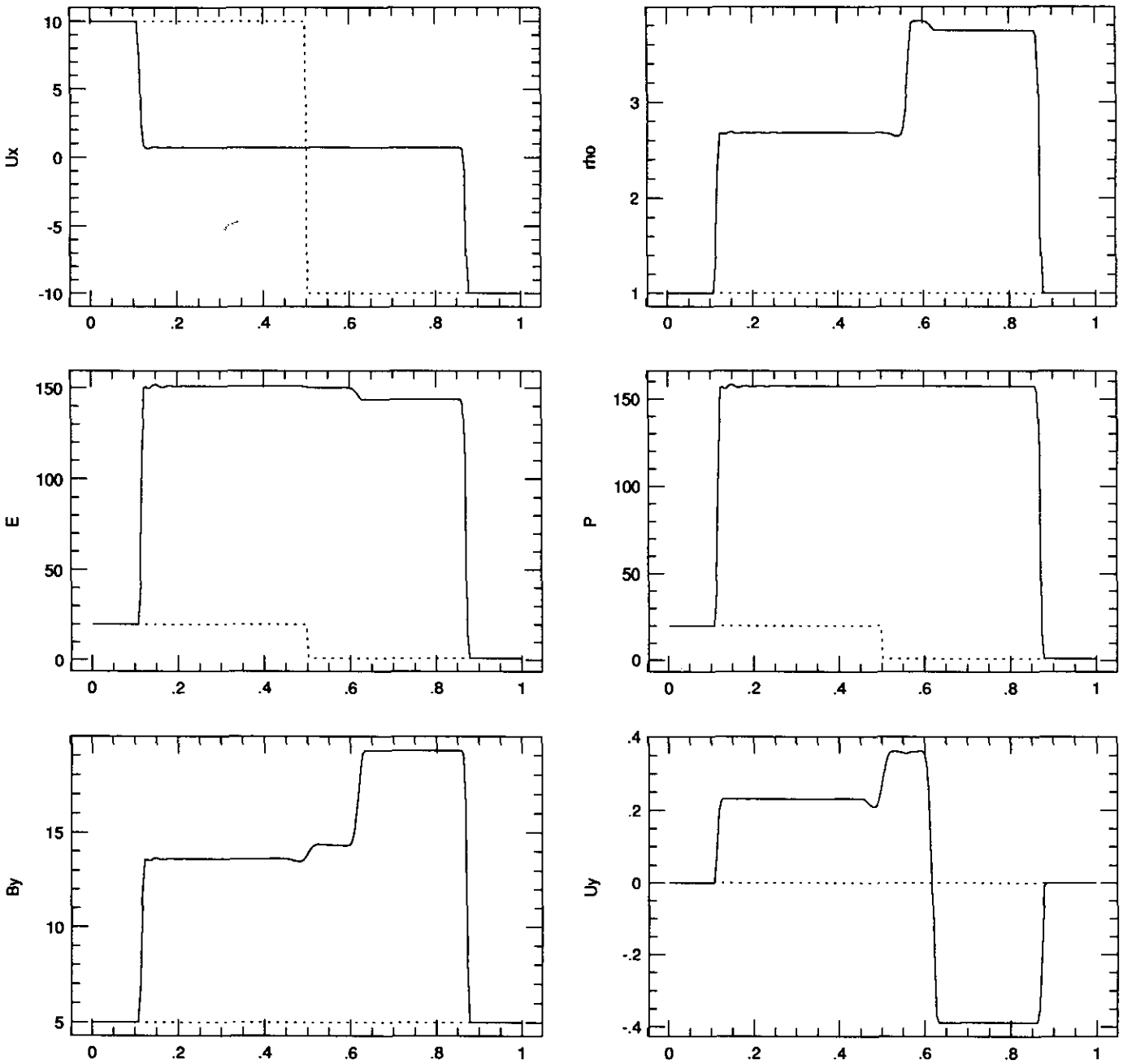

FIG. 8. The profiles in a 1D MHD computer simulation with the left and right states $(\rho, p, u_x, u_y, u_z, B_y, B_z)_L = (1, 20, 10, 0, 0, 5, 0)$ and $(\rho, p, u_x, u_y, u_z, B_y, B_z)_R = (1, 2, -10, 0, 0, 5, 0)$ with $B_x = 5$ and $\gamma = \frac{5}{3}$. 200 numerical zones are used in the simulation. The dashed lines are the initial condition, and the solid lines are the profiles at $t = 0.08$.

solver could not solve the Riemann problem successfully with the initial guess. In MHD simulations we simply give the average values of the left and right states for fluxes if the Riemann solver fails at any specific interface and at any specific time. Figure 8 shows one strong fast shock propagating to the right, one fast shock moving to the left, one contact discontinuity, and one weak slow shock.

In some applications of MHD, people are interested in two-dimensional phenomena, and in the fast shocks and the slow shocks, but not in the rotational discontinuities. Thus an MHD Riemann solver for the flow with two components is needed. Most of the work reported above is also valid for these applications with some necessary changes in formulae. In the remaining part of this section, we will make the changes to present an approximate Riemann solver for these applications. We will suppose that there are no z-components of the magnetic field and flow velocity in the following part of this section.

It is known that the system permits the fast and slow waves only. The Alfven wave is excluded from the system since the restriction of only two instead of three components is applied. The perturbation $\delta\mathbf{B}$ in magnetic field $\mathbf{B}$ is perpendicular to both the magnetic field and the direction of wave propagation for Alfven waves. For this reason, Alfven waves are the three-component phenomena. They can be seen in two-component systems only in the special case with the direction of the propagation aligned with the magnetic field. All the formulae for the fast and slow wave speeds and their associated Riemann invariants given in the third section are still valid by simply setting $B_z = u_z = 0$.

For flows with discontinuities, the relations between the jumps across the shock front and the shock speed, Eq. (6) and Eq. (9), are also true if the parameter λ is set to be zero. With these relations, we construct the procedures of the Riemann solver for two-component simulations by the following procedures:

(1) Guess the transverse component of the magnetic field B_{y2}, B_{y4}, and B_{y7} in regions R2, R4, and R7, and R7, and let B_{y5} equal B_{y4}.

(2) Calculate two possible fast shock speeds in both directions, then apply the jump conditions to obtain the complete states in regions R2 and R7, respectively.

(3) Let the state in regions R3 and R5 equal the states in regions R2 and R7 since there is no rotational discontinuity involved.

(4) Repeat procedure (2) for two possible slow shocks to obtain two slow shock speeds and the states in regions R4 and R5.

(5) Use the conditions for a contact discontinuity between the regions R4 and R5 $u_{x4} = u_{x5}$, $u_{y4} = u_{y5}$, and $p_4 = p_5$ to improve the earlier guess on the magnetic field in regions R2, R4, and R7; then go back to the procedure (1).

6. SUMMARY AND DISCUSSION

To find an efficient Godunov-type scheme for compressible MHD with strong discontinuities is the main motivation of this work. The necessary ingredients for such a scheme include upstream centering for all Riemann invariants, a correct weak-wave limit, and some degree of nonlinearity for strong shocks. The MHD Riemann solver presented in this paper is designed mainly for the calculation of time-averaged fluxes at the interfaces of numerical zones. Our main concern for the MHD Riemann solver is that it produces reasonable solutions obeying all conservation laws for any pair of left and right states, but our MHD Riemann solver need not give exact solutions. The numerical method we want to develop should work for all kinds of the discontinuities in ideal MHD, including fast shocks, slow shocks, rotational discontinuities, tangential discontinuities, and contact discontinuities. We believe that one of the main difficulties in this task is solving the Riemann problem in ideal MHD in an appropriate approximation. The problem is that the solution of the ideal MHD Riemann problem is not unique. We have chosen the branch of solutions which takes a correct weak-wave limit and the Riemann invariants from their proper domains and incorporates them in a reasonable fashion of the nonlinear jump conditions for strong discontinuous waves.

In order to solve the Riemann problem approximately, we have investigated all the discontinuities in MHD. We have found that the three component model is necessary for the MHD Riemann problem to display all the discontinuities. The compound wave reported in the earlier work disappears in our solutions from the MHD Riemann solver, but it will be generated through the conservation law, Eqs. (2.1)–(2.7), no matter what approximation we use in the calculation of time-averaged fluxes at the interfaces of the numerical zones if the conditions of the flow demand its appearance. Even if we are given such left and right states in which there are no third components of both the magnetic field and the flow velocity, the solutions of the Riemann problem may involve rotational discontinuities. In order to develop an efficient Riemann solver for MHD, we have found completely nonlinear formulae for both fast and slow shock speeds in terms of their pre-shock states and one variable at their post-shock states. We have also obtained formulae for the jumps across a shock in terms of the shock speed and the pre-shock state.

Based on these results about shocks and rotational discontinuities, a nonlinear approximate MHD Riemann solver has been constructed. It consists of the initial guess, the calculation of two shock speeds and two post-shock states for two possible fast shocks, the performance of rotations, the calculation of two slow shock speeds and their post-shock states and the improvement of the initial guess. This Riemann solver separates all the possible discon-

tinuities in MHD from the initial single discontinuity. The solutions of a general Riemann problem in ideal MHD involve two fast waves (either shock or rarefaction), two rotational discontinuities with different angles rotated, two slow waves (either shock or rarefaction), and one contact discontinuity. We have given solutions for several typical MHD Riemann problems which involve multiple strong discontinuities.

In order to make the initial guess properly, we have given equations for seven characteristics and their associated Riemann invariants. Based on the theory of characteristics and Riemann invariants, a linear Riemann solver has been given in the first part of the paper. The linear Riemann solver is valid only for infinitesimal jumps, but is also used in the initial guess in the nonlinear Riemann solver. An alternative for the initial guess from the linear Riemann solver is suggested which appropriately chooses the value at the left or right state as the initial guess assuming that there is only one strong discontinuity and some other weak discontinuities. For some left and right states, which involve multiple strong discontinuities, a relaxation method is used.

We start from the jump conditions, the conservation laws across any discontinuity surface. We expect this technique works well for MHD shock dynamics, but limits the application of the Riemann solver to weak rarefactions. An appropriate initial guess is critical for this Riemann solver for some MHD Riemann problems which involve multiple strong discontinuities.

Although the Riemann solver may be put to more sophisticated use through enough iterations, its main application will be the calculation of the fluxes in a Godunov-type scheme. For most problems in MHD, we find that one iteration is enough to obtain sufficiently accurate fluxes in an actual code even for very strong MHD shocks. Such examples of the calculation may be found in our subsequent paper. Without any optimization, the Riemann solver with one iteration in our current one-dimensional code may solve 348,143 Riemann problems per second on a Cray-C90 machine. The complexity of the Riemann solver is determined by the MHD equations. The most efficient implementation of the Riemann solver in a Godunov-type scheme remains to be found. The cost of the Riemann solver in an actual code may be reduced. For example, only in a part of the simulation domain is the nonlinear Riemann solver needed, and in the other part, our linear Riemann solver is enough to give a reasonable solution for the fluxes. The cost of the Riemann solver in an actual code depends on efficient use of the Riemann solver and on a specific problem which determines the necessary part of the simulation domain for use of the nonlinear Riemann solver. Therefore, the cost of the Riemann solver should be reported in the actual simulation for a specific problem.

ACKNOWLEDGMENTS

We acknowledge useful discussions with Professor Thomas W. Jones. The work reported here has also built upon the earlier work of Giz and Woodward reported in Refs. [13, 21]. This work was mainly supported by the U.S. Department of Energy through Grant DE-FG02-87ER25035 and was supported in part by the Army Research Office Contract DAAL03-89-C-0038 with the University of Minnesota Army High Performance Computing Research Center.

REFERENCES

1. S. K. Godunov, *Math. Sb.* **47**, 271 (1959).
2. B. Van Leer, *J. Comput. Phys.* **32**, 101 (1979).
3. B. van Leer and P. R. Woodward, in *Proceedings TICOM Conference, Austin, Texas, 1979.*
4. P. R. Woodward and P. Collela, *Lecture Notes in Physics*, Vol. 141 (Springer-Verlag, New York/Berlin, 1981), p. 434.
5. P. L. Roe, *J. Comput. Phys.* **43**, 358 (1981).
6. A. Harten, *J. Comput. Phys.* **49**, 357 (1983).
7. P. R. Woodward and P. Colella, *J. Comput. Phys.* **54**, 115 (1984).
8. P. Colella and P. R. Woodward, *J. Comput. Phys.* **54**, 174 (1984).
9. P. Colella, *SIAM J. Sci. Stat. Comput.* **6**(1), 104 (1985).
10. A. Harten, S. Osher, B. Engquist, and S. Chakravarthy, *J. Appl. Numer. Math.* **2**, 347 (1986).
11. A. Harten and S. Osher, *SIAM J. Numer. Anal.* **24**, 279 (1987).
12. A. Harten, B. Engquist, S. Osher, and S. Chakravarthy, *J. Comput. Phys.* **71**, 231 (1987).
13. A. T. Giz, Ph.D. thesis, University of California, Berkeley, 1987.
14. C. C. Wu, *Geophys. Res. Lett.* **14**, 668 (1987).
15. C. C. Wu, *J. Geophys. Res.* **93**, 3969 (1988).
16. M. Brio and C. C. Wu, *J. Comput. Phys.* **75**, 400 (1988).
17. M. Brio, in *Nonlinear Hyperbolic Equations—Theory, Computation Methods, and Applications: Proceedings, Second International Conference on Nonlinear Hyperbolic Problems, Aachen, FRG, March 14–18, 1988.*
18. J. Glimm, in *Nonlinear Hyperbolic Equations—Theory, Computation Methods, and Applications: Proceedings, Second International Conference on Nonlinear Hyperbolic Problems, Aachen, FRG, March 14–18, 1988.*
19. J. B. Bell, P. Colella, and J. A. Trangenstein, *J. Comput. Phys.* **82**, 362 (1989).
20. C. C. Wu, *J. Geophys. Res.* **95**, 8149 (1990).
21. A. T. Giz and P. R. Woodward, *Turkish J. Phys.* **16**, 353 (1992).
22. A. L. Zachary and P. Collela, *J. Comput. Phys.* **99**, 341 (1992).
23. L. D. Landau and E. Lifshits, *Electrodynamics of Continuous Media* (Pergamon, New York, 1960).
24. R. Courant and K. O. Friedrichs, *Supersonic Flow and Shock Wave*, 5th ed. (Interscience, New York, 1967).
25. B. L. Keyfitz and H. C. Kranzer (Eds.), *Nonstrictly Hyperbolic Conservation Laws, 12th Proceedings of AMS Special Session, Anaheim, CA, January 9–10, 1985.*
26. A. Jeffrey and T. Taniuti, *Non-linear Wave Propagation* (Academic Press, New York/London, 1964).
27. A. G. Kulikovskiy and G. A. Lyubimov, *Magnetohydrodynamics* (Addison–Wesley, Reading, MA, 1965).
28. A. R. Kantrowitz and H. E. Petscheck, in *Plasma Physics in Theory and Application* (McGraw–Hill, New York, 1966).